Composition Dependence of Structural and Electronic Properties of Quaternary InGaNBi

Liang *et al. Nanoscale Research Letters* (2019) 14:178
https://doi.org/10.1186/s11671-019-2968-0

Nanoscale Research Letters

NANO EXPRESS Open Access

Composition Dependence of Structural and Electronic Properties of Quaternary InGaNBi

Dan Liang[1], Pengfei Zhu[1], Lihong Han[1], Tao Zhang[2], Yang Li[1], Shanjun Li[2*], Shumin Wang[3,4] and Pengfei Lu[1*]

Abstract

To realize feasible band structure engineering and hence enhanced luminescence efficiency, InGaNBi is an attractive alloy which may be exploited in photonic devices of visible light and mid-infrared. In present study, the structural, electronic properties such as bandgap, spin-orbit splitting energy, and substrate strain of InGaNBi versus In and Bi compositions are studied by using first-principles calculations. The lattice parameters increase almost linearly with increasing In and Bi compositions. By bismuth doping, the quaternary InGaNBi bandgap could cover a wide energy range from 3.273 to 0.651 eV for Bi up to 9.375% and In up to 50%, corresponding to the wavelength range from 0.38-1.9 μm. The calculated spin-orbit splitting energy are about 0.220 eV for 3.125%, 0.360 eV for 6.25%, and 0.600 eV for 9.375% Bi, respectively. We have also shown the strain of InGaNBi on GaN; it indicates that through adjusting In and Bi compositions, InGaNBi can be designed on GaN with an acceptable strain.

Keywords: Quaternary, InGaNBi, First-principles, Electronic, Strain

Introduction

In recent years, wurtzite (WZ) $In_xGa_{1-x}N$ alloys and InGaN/GaN quantum wells (QWs) have aroused wide attention due to their large potential for developing solar cells, high-efficiency light emitting diodes (LEDs), and laser diodes (LDs) [1–10]. The commonly used [0001]-oriented $In_xGa_{1-x}N$/GaN QWs suffer an intense built-in electric field induced by biaxial compressive stress of the $In_xGa_{1-x}N$ layer [11], which gives rise to the decrease in QW emission energy and oscillator strength of electron-hole pairs. Besides, there exists a high-density of geometric defects in $In_xGa_{1-x}N$ alloys, including stacking faults and threading dislocations (TDs) [12]; these TDs have a large correlation with non-radiative recombination centers. Defects, electron leakage, and Auger recombination are the three sources for the efficiency droop of $In_xGa_{1-x}N$ LEDs, of which the Auger recombination is the principal cause [13].

Similarly, for GaAs-based infrared diodes, it has already been proposed that bismuth alloying is an effective method to decrease bandgap (E_g) as well as enhance spin-orbit (SO) splitting to achieve the suppression of Auger recombination process [14]. The largest group V element of bismuth reveals attractive effects on physical properties of bismide alloys. The changes in the band structure of bismide alloys have been investigated for different ternary alloy materials both experimentally and theoretically, such as AlNBi [15], GaNBi [16, 17], GaSbBi [18, 19], InPBi [20, 21], and InSbBi [19, 22–24]. The bandgap is modified mainly by the large Bi atom-induced strain at high concentration in InPBi. The incorporation of Bi perturbs the valence bands (VBs) due to the interaction of Bi impurity states with heavy/light hole bands and spin-orbit split off bands [21]. More recently, quaternary bismide alloys (for example, GaAsNBi [25–27], InGaAsBi [28, 29], GaAsPBi [30]) have also garnered extensive attention. The local distortions around P and Bi atoms significantly contribute to the bandgap modification of GaAsPBi. A composition requirement for $GaAs_{1-x-y}P_yBi_x$ to achieve lower

*Correspondence: lishanjun@scu.edu.cn; photon.bupt@gmail.com
[1]State Key Laboratory of Information Photonics and Optical Communications, Beijing University of Posts and Telecommunications, 100876 Beijing, China
[2]College of Electrical Engineering and Information Technology, Sichuan University, 610065 Chengdu, China
Full list of author information is available at the end of the article

Auger recombination ratio than GaAs was obtained [30]. Combining bismuth and other III or V atom increases the scope of band structure engineering, including control of bandgap, spin-orbit splitting, conduction (CB) and valence band offsets, and strain [25]. Therefore, it is of significant interest to describe the effect of Bi substitution on the [0001] In_xGa_{1-x}N/GaN, tuning the structural and electronic properties and hence the luminescence efficiency. In present study, using first-principles calculations [31], the structural, electronic properties such as bandgap, spin-orbit splitting energy (Δ_{SO}), and substrate strain of InGaNBi versus In and Bi compositions are studied. Considering the large lattice mismatch and poor quality for In content higher than 55–60% in InGaN sample [32] as well as the low solubility of bismuth in diluted-bismide alloys, the concentrations of In and Bi are controlled up to 50% and 9.375%, respectively. The paper is organized as follows. In the "Methods" section, we present the detailed computational methods. The structural, electronic properties and substrate strain are provided in the "Results and Discussion" section. Finally, a short summary is summarized.

Methods

Our theoretical calculations are based on the density functional theory (DFT) [31] as implemented in the VASP code [33, 34]. In the calculations of structural properties, the electron-ion and exchange-correlation interactions are treated with the projector augmented wave method (PAW) [35, 36] and the generalized gradient approximation (GGA) of the Perdew-Burke-Ernzerhof (PBE) [37], respectively. The valence-electron configurations for In, Ga, N, and Bi atoms are employed as $4d^{10}5s^25p^1$, $3d^{10}4s^24p^1$, $2s^22p^3$, and $5d^{10}6s^26p^3$, respectively. In order to overcome the underestimation of PBE potential on the bandgap of the electronic properties, we employ the modified Becke-Johnson exchange potential in combination with local density approximation correlation (MBJLDA) [38]. Bismuth has a large spin-orbit coupling (SOC) effect, and therefore, SOC is included in the electronic calculations. In all the computations, the structures are relaxed until the forces on each atom become less than 0.02 eV/Å and maximum energy change is of the order of 10^{-4} eV. A plane-wave cutoff of 450 eV is set to ensure the accuracy of the calculations. A Monkhorst-Pack of $4 \times 4 \times 4$ k-point mesh is adopted in the first Brillouin zone.

Results and Discussion

Structural Properties

The supercells consist of $4 \times 2 \times 2$ of WZ-GaN primitive cell, including 64 atoms. We investigate 36 compositions of $In_yGa_{1-y}N_{1-x}Bi_x$ with $0 \leq x \leq 0.09375, 0 \leq y \leq 0.5$ based on recent experiments where InGaN sample exhibits large lattice mismatch and poor quality for In content higher than 55–60% [32] as well as the low solubility of bismuth in diluted-bismide alloys. One representative configuration is considered where In and Bi atoms are evenly spread out. We have summarized the calculated lattice parameters of ternary In_yGa_{1-y}N and quaternary $In_yGa_{1-y}N_{1-x}Bi_x$ alloys together with other theoretical and experimental data in Fig. 1. For pristine GaN, the lattice parameters $a = 3.211$, $c = 5.235$ Å, which are in good agreement with other theoretical calculations $a = 3.155, 3.22$ Å, $c = 5.144, 5.24$ Å [39–41] and experimental data 3.19 Å for a, 5.19 Å for c [42]. The lattice parameters (a, c) of In_yGa_{1-y}N rise when In composition is increased and show a nearly linear variation, as shown in Fig. 1a. The present calculations predict $a = 3.304$ Å, $c = 5.365$ Å for $In_{0.25}$GaN and $a = 3.397$ Å, $c = 5.509$ Å for $In_{0.5}$GaN, all of which agree well with previous results of a = 3.33 Å, c = 5.39 Å for $In_{0.25}$GaN and $a = 3.43, 3.485$ Å, $c = 5.55, 5.488$ Å for $In_{0.5}$GaN [39, 40, 43, 44]. In the case of quaternary alloys $In_yGa_{1-y}N_{1-x}Bi_x$, as far as we are concerned, there are no experimental and theoretical values for structural properties. In Fig. 1b, the obtained lattice parameters also increase almost linearly with increasing In and Bi compositions. Because of larger ionic radii of In and Bi than Ga and N atoms, the substitution of In over Ga and Bi over N leads enhanced lattice parameters of InGaNBi.

In and Bi incorporation will break the crystal periodicity and introduce geometrical deformation in a heavily alloyed structure. We choose $In_{0.25}GaNBi_{0.0625}$ as an example for four chemical bonds statistics, as shown in Fig. 2; the average lengths of the Ga-N, In-N, Ga-Bi, and In-Bi bonds are 2.009, 2.195, 2.592, and 2.704 Å, respectively. Note that the Ga-N bond length in pristine bulk GaN is 1.970 Å. The In-N bond length is larger than that of Ga-N, which indicates In atom markedly pushes N atom away. Similarly, the larger bond length of Ga-Bi than Ga-N means Bi atom pushes Ga atom away, finding good consistency with the order of covalent radii of Ga (1.22 Å), In (1.42 Å), N (0.71 Å), and Bi (1.48 Å) [45]. Other configurations display the similar behavior. Lattice deformation and disparity in electronegativity between the host and dopant have considerable effect on electronic and optical properties.

Electronic Properties

It has been shown that the functional or correction potentials and SOC effect greatly influence the predicted accuracy of III-V alloy bandgap energy, valence band, and spin-orbit splitting energy. Thus, we validate our results using MBJLDA potential and compare with other theoretical calculations and experiments. Figure 3 is a plot of bandgap energy versus In composition in In_yGa_{1-y}N as well as a fit to the data. Some bandgap values obtained by

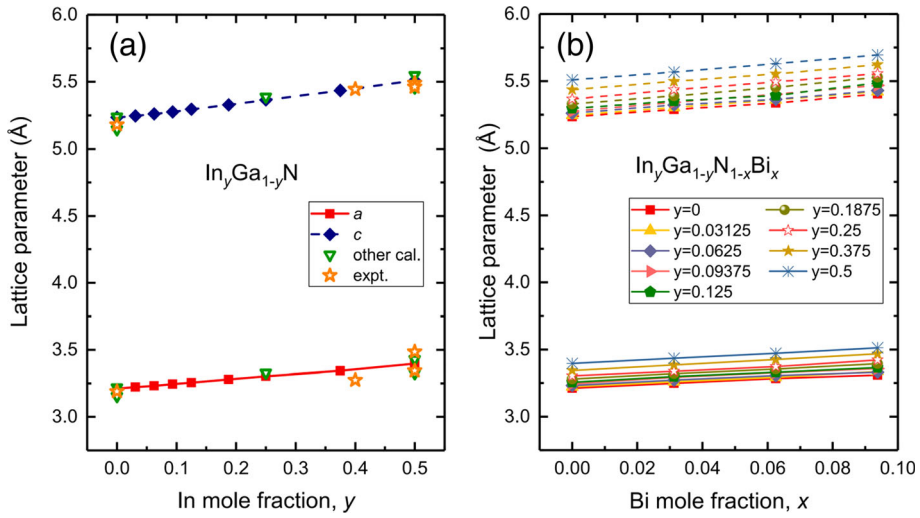

Fig. 1 The lattice parameters for **a** ternary alloys $In_yGa_{1-y}N$, with $0 \leq y \leq 0.5$ and **b** quaternary alloys $In_yGa_{1-y}N_{1-x}Bi_x$, with $0 \leq x \leq 0.09375$, $0 \leq y \leq 0.5$. For comparison, we add some other calculations and experimental data from Ref. [39–44] in Fig. 1a. The solid line represents *a* and dashed line is *c*

experiments, theoretical HSE06, mBJ, and LMTO-CPA-MBJ functionals are also plotted. The predicted bandgap of GaN is 3.273 eV, which is in good consistency with present calculations and experiments, 3.33 eV by mBJ [40], 3.261, 3.23 eV by HSE06 [39, 46], and 3.40–3.50 eV by experiments [47–49]. As observed in $In_yGa_{1-y}N$, our DFT results confirm that E_g values of $In_yGa_{1-y}N$ continuously decrease as y is increased from 0 to 50%. E_g smoothly decreases from 3.273 to 1.546 eV. This compares well with those from theoretical (HSE06, mBJ potentials)[39, 40, 46] and experimental results [50, 51].

The contour plot for the bandgap of quaternary $In_yGa_{1-y}N_{1-x}Bi_x$ alloys is shown in Fig. 4. The bandgaps of the quaternary alloys display a non-linear trend as a function of composition, which decreases with increasing In and Bi contents. From the results, we find that InGaNBi bandgap could cover a wide energy range from 3.273 to 0.651 eV for Bi up to 9.375% and In up to 50%, corresponding to the wavelength range from 0.38 to 1.9 μm,

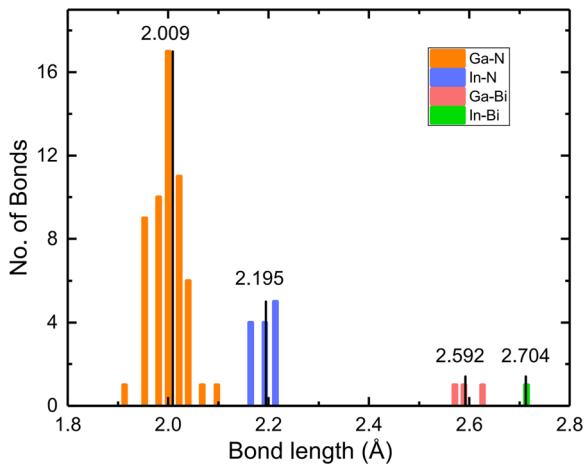

Fig. 2 Histogram of bond length in $In_{0.25}GaNBi_{0.0625}$. The values in panel indicate the average lengths of the four types of bond

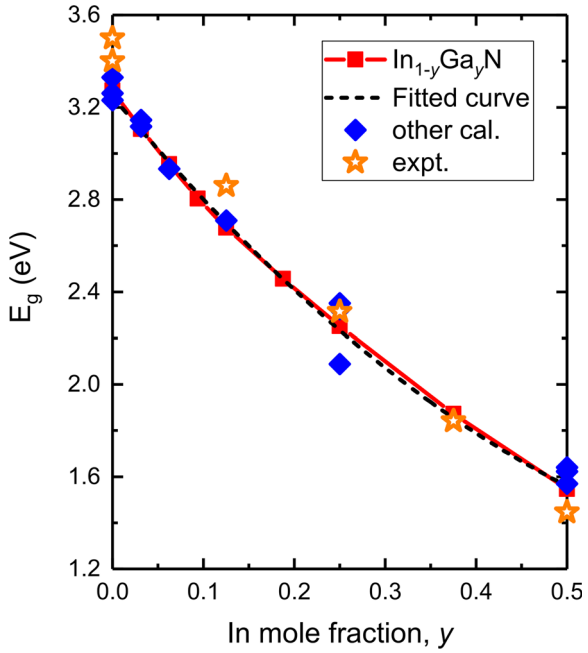

Fig. 3 Predicted bandgap energy (E_g, red solid line) as a function of In composition in $In_yGa_{1-y}N$ as well as a fit to the data (black dashed line). Other theoretical [39, 40, 46] and experimental [47–51] results are also plotted

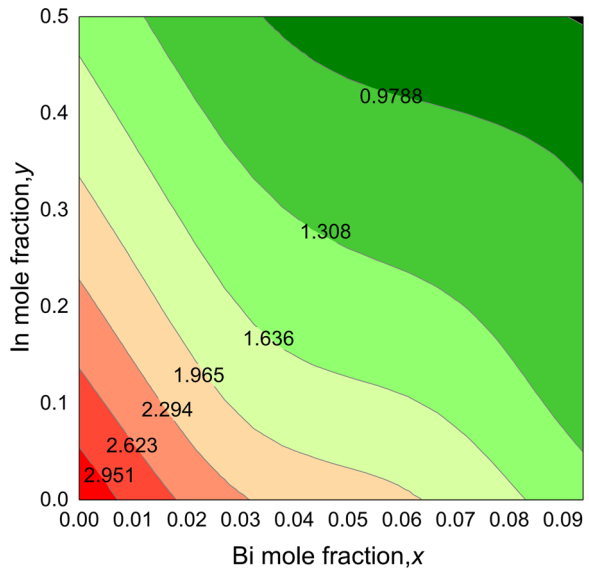

Fig. 4 Contour plot of the bandgap values for $In_yGa_{1-y}N_{1-x}Bi_x$ alloys, as a function of Bi(x) and In(y) compositions

indicating their potential optoelectronic applications in visible light and mid-infrared scope.

Compared with InGaN, the incorporation of Bi induces a sharper bandgap reduction. But beyond that, a significant increase in Δ_{SO} is obtained due to the strong SOC effect of bismuth where the advanced interaction between the electron spin and orbital angular momentum decreases the SO band energy. Furthermore, the improved valence-band edge arised from the valence band anti-crossing effect of bismide alloys also largely enhances Δ_{SO} [28]. Our calculated Δ_{SO} values are about 0.220 eV for 3.125%, 0.360 eV for 6.25%, and 0.600 eV for 9.375% Bi, respectively, which has an insignificant variation with indium fraction. Previous investigations have demonstrated that different Bi arrangements are of great influence on band structures of bismide alloys, including spin-orbit splitting energy [21, 52]. The present results display that the $In_{0.5}GaNBi_{0.09375}$ bandgap value (0.651 eV) is very close to that of Δ_{SO} (0.577 eV). Since InGaN sample exhibits large lattice mismatch and poor quality for In content higher than 55–60% [32] as well as the low solubility of bismuth in diluted-bismide alloys, we set the contents of In up to 50% and Bi up to 9.375%. We believe that a higher indium or bismuth content will achieve $\Delta_{SO} > E_g$ in quaternary InGaNBi sample to enhance the efficiency of InGaNBi-based LEDs and LDs.

The projected band structures and total density of states (TDOS) of pristine GaN, $In_{0.25}$GaN, and $In_{0.25}GaNBi_{0.03125}$ alloys are presented in Fig. 5. The contributions of In and Bi are highlighted by color: blue (red) corresponds to the state originating from In (Bi). The In substitution in $In_{0.25}$GaN has great influence on both the conduction band and valence band, where the conduction band minimum (CBM) is pushed to lower energies regarding the Fermi level and reflect narrower energy gap. Unlike bismuth that introduces the defect band in the forbidden gap near the Fermi level, the In atoms show a hybridization with the deep level of the VB. For quaternary alloy $In_{0.25}GaNBi_{0.03125}$, it can be clearly seen that the reduction of bandgap results from both upward valence band maximum (VBM) and downward CBM, and CBM changes more significantly compared to $In_{0.25}$GaN, which is attributed to larger compressive strain in InGaNBi from the addition of bismuth. The defect level highlighted by red color has a strong interaction with the VB edge, which is derived from the hybridization mainly between Bi and the near Ga atoms. The TDOS in Fig. 5e also reflects the local defect level at −1.0 to −0.5 eV.

Strain of InGaNBi on GaN

The [0001]-oriented In_yGa_{1-y}N/GaN strained quantum wells are widely adopted in current LED and LD devices, in which In_yGa_{1-y}N layers suffer a biaxial compressive stress. Local compositional fluctuations and different covalent radii of In and Ga atoms give rise to the strains in In_yGa_{1-y}N layers [53]. Figure 6 shows the strain of InGaNBi on an GaN substrate. Since indium atom is larger than gallium atom, bismuth atom is larger than nitrogen atom; thus, incorporating In and Bi atoms in InGaNBi induces compressive strain InGaNBi on GaN. It is shown that in the In content of 50% and Bi content of 9.375%, InGaNBi is under high 8.5% compressive strain. For In fraction within 6.25% and Bi fraction within 2.8%, the strain of InGaNBi on GaN is within 1%. That is, through adjusting In and Bi compositions, InGaNBi can be designed on GaN with an acceptable strain.

Conclusions

The structural, electronic properties and strain of InGaNBi on GaN versus In and Bi compositions are investigated based on density functional theory. The lattice parameters of InGaNBi increase almost linearly with increasing In and Bi compositions. Since In and Bi atoms have the larger atomic radius than that of Ga and N atoms, the In-N and Ga-Bi bond lengths are larger than that of Ga-N. For electronic properties, we have shown the contour plot for the bandgap of quaternary $In_yGa_{1-y}N_{1-x}Bi_x$ alloys. The quaternary alloys bandgap could cover a wide energy range from 3.273 to 0.651 eV for Bi up to 9.375% and In up to 50%, corresponding to the wavelength range from 0.38 to 1.9 μm. The calculated Δ_{SO} values are about 0.220 eV for 3.125%, 0.360 eV for 6.25%, and 0.600 eV for 9.375% Bi, respectively, which has an insignificant variation with indium fraction. We believe that a higher

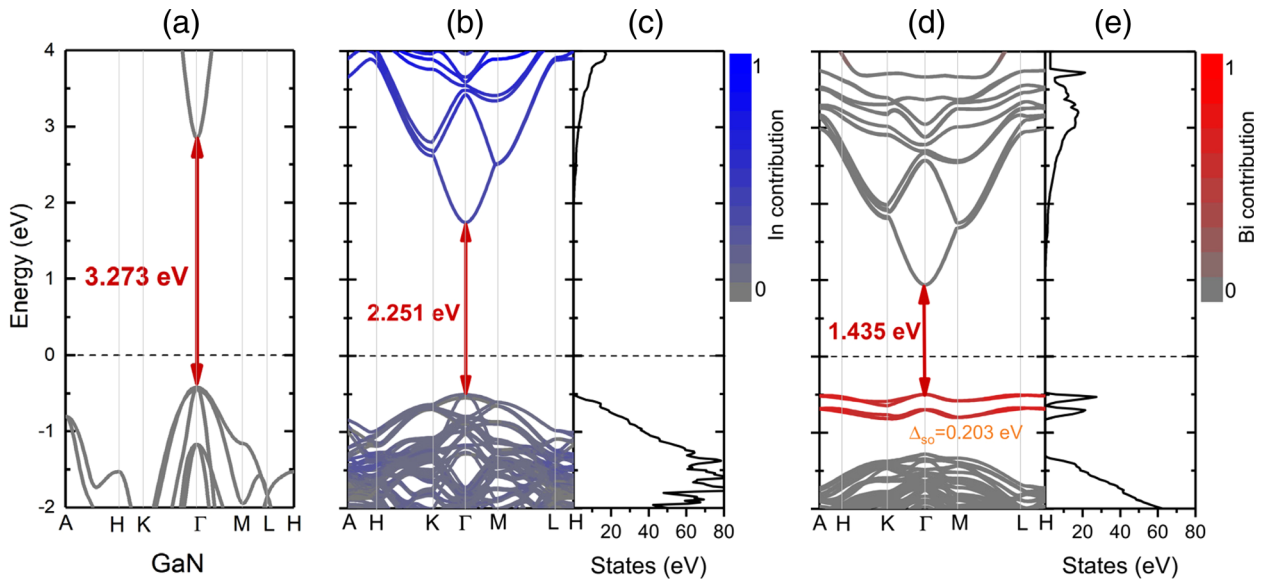

Fig. 5 The projected band structures and their corresponding total density of states (TDOS) of **a** GaN, **b**, **c** $In_{0.25}GaN$, and **d**, **e** $In_{0.25}GaNBi_{0.03125}$. The black dashed line represents the Fermi level, which sets to be zero. The relative contributions of In and Bi are highlighted by color: blue (red) corresponds to the state originating from In (Bi)

indium or bismuth composition will achieve $\Delta_{SO} > E_g$ in quaternary InGaNBi sample to enhance the efficiency of InGaNBi-based LEDs and LDs. The band structure analyses show the indium has great influence on both CB and VB, and bismuth has a strong interaction with the VB edge. Finally, we investigate the strain of InGaNBi on GaN. Through adjusting In and Bi compositions, InGaNBi can be designed on GaN with an acceptable strain.

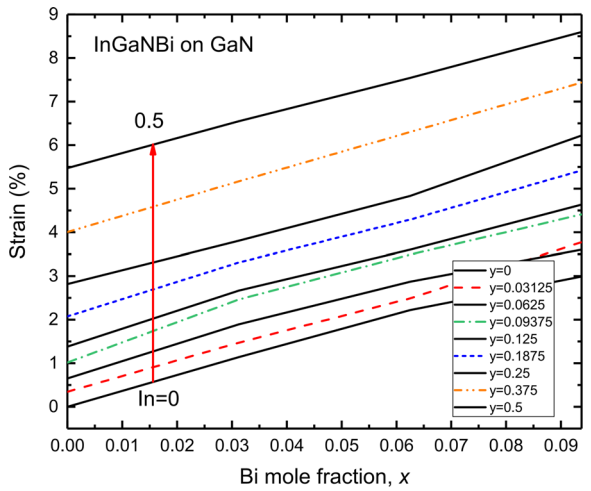

Fig. 6 Strain of InGaNBi alloys on GaN substrate at various In (0–0.5) as a function of Bi fraction. Positive values of strain indicate InGaNBi is under compressive strain

Acknowledgements
This work was supported by the National Key Research and Development Program of China (No.2018YFB0406601), the National Natural Science Foundation of China (Nos.61675032), the BUPT Excellent Ph.D. Students Foundation (CX2017202), the State Scholarship Fund (201806470066) from China Scholarship Council, and the Open Program of State Key Laboratory of Functional Materials for Informatics. We also acknowledge the computational support from the Beijing Computational Science Research Center (CSRC).

Authors' Contributions
DL and PZ performed the calculations. LH, TZ, YL, and SW analyzed the data. PL and SL supervised the research. DL, PZ, and YL wrote the manuscript and prepared the figures. All authors reviewed the manuscript. All authors read and approved the final manuscript.

Competing Interests
The authors declare that they have no competing interests.

Publisher's Note

Author details
[1]State Key Laboratory of Information Photonics and Optical Communications, Beijing University of Posts and Telecommunications, 100876 Beijing, China. [2]College of Electrical Engineering and Information Technology, Sichuan University, 610065 Chengdu, China. [3]State Key Laboratory of Functional Materials for Informatics, Shanghai Institute of Microsystem and Information Technology, Chinese Academy of Sciences, 200050 Shanghai, China. [4]Photonics Laboratory, Department of Microtechnology and Nanoscience, Chalmers University of Technology, 41296 Gothenburg, Sweden.

Received: 20 December 2018 Accepted: 1 April 2019
Published online: 28 May 2019

References

1. Neufeld CJ, Toledo NG, Cruz SC, Iza M, DenBaars SP, Mishra UK (2008) High quantum efficiency InGaN/GaN solar cells with 2.95 eV band gap. Appl Phys Lett 93(14):143502

2. Chen X, Matthews KD, Hao D, Schaff WJ, Eastman LF (2008) Growth, fabrication, and characterization of InGaN solar cells. Phys Status Solidi (a) 205(5):1103–1105
3. Wu J (2009) When group-III nitrides go infrared: new properties and perspectives. J Appl Phys 106(1):011101
4. Wang Q, Li X, Wu L, Lu P, Di Z (2019) Electronic and interface properties in graphene oxide/hydrogen-passivated Ge heterostructure. Phys Status Solidi-R 13(2):1800461
5. Wu L, Lu P, Quhe R, Wang Q, Yang C, Guan P, Yang K (2018) Stanene nanomeshes as anode materials for Na-ion batteries. J Mater Chem A 6(17):7933–7941
6. Guo L, Deng J, Wang G, Hao Y, Bi K, Wang X, Yang Y (2018) N, P-doped CoS_2 embedded in TiO_2 nanoporous films for Zn-air batteries. Adv Funct Mater 28(42):1804540
7. Bi K, Bi M, Hao Y, Luo W, Cai Z, Wang X, Huang Y (2018) Ultrafine core-shell $BaTiO_3@SiO_2$ structures for nanocomposite capacitors with high energy density. Nano Energy 51:513–523
8. Yang H, Geng L, Zhang Y, Chang G, Zhang Z, Liu X, Lei M, He Y (2019) Graphene-templated synthesis of palladium nanoplates as novel electrocatalyst for direct methanol fuel cell. Appl Surf Sci 466:385–392
9. Wang H, et al (2018) Durable and efficient hollow porous oxide spinel microspheres for oxygen reduction. Joule 2(2):337–348
10. Liang D, et al (2017) Electronic and excitonic properties of two-dimensional and bulk InN crystals. RSC Adv 7(67):42455–42461
11. Shi J, Gan Z (2003) Effects of piezoelectricity and spontaneous polarization on localized excitons in self-formed InGaN quantum dots. J Appl Phys 94(1):407–415
12. Chichibu SF, et al (2006) Origin of defect-insensitive emission probability in In-containing (Al,In,Ga)N alloy semiconductors. Nat Mater 5(10):810–816
13. Iveland J, Martinelli L, Peretti J, Speck JS, Weisbuch C (2013) Direct measurement of auger electrons emitted from a semiconductor light-emitting diode under electrical injection: identification of the dominant mechanism for efficiency droop. Phys Rev Lett 110(17):177406
14. Batool Z, Hild K, Hosea TJC, Lu X, Tiedje T, Sweeney SJ (2012) The electronic band structure of GaBiAs/GaAs layers: influence of strain and band anti-crossing. J Appl Phys 111(11):113108
15. Mbarki M, Alaya R, Rebey A (2013) Ab initio investigation of structural and electronic properties of zinc blende Al$N_{1-x}Bi_x$ alloys. Solid State Commun 155:12–15
16. Mbarki M, Rebey A (2012) First principles calculations of structural and electronic properties of Ga$N_{1-x}Bi_x$ alloys. J Alloy Compd 530:36–39
17. Levander AX, Yu KM, Novikov SV, Tseng A, Foxon CT, Dubon OD, Wu J, Walukiewicz W (2010) Ga$N_{1-x}Bi_x$: extremely mismatched semiconductor alloys. Appl Phys Lett 97(14):141919
18. Polak MP, et al (2014) Theoretical and experimental studies of electronic band structure for $GaSb_{1-x}Bi_x$ in the dilute Bi regime. J Phys D Appl Phys 47(35):355107
19. Polak MP, Scharoch P, Kudrawiec R (2015) First-principles calculations of bismuth induced changes in the band structure of dilute Ga-V-Bi and In-V-Bi alloys: chemical trends versus experimental data. Semicond Sci Tech 30(9):094001
20. Wang K, Gu Y, Zhou HF, Zhang LY, Kang CZ, Wu MJ, Pan WW, Lu PF, Gong Q, Wang SM (2014) InPBi single crystals grown by molecular beam epitaxy. Sci Rep 4:5449
21. Chen X, Shen W, Liang D, Quhe R, Wang S, Guan P, Lu P (2018) Effects of Bi on band gap bowing in In$P_{1-x}Bi_x$ alloys. Opt Mater Express 8(5):1184–1192
22. Lee JJ, Kim JD, Razeghi M (1997) Long-wavelength infrared photodetectors based on InSbBi grown on GaAs substrates. Appl Phys Lett 71(16):2298–2300
23. Das SC, Das TD, Dhar S (2012) Infrared absorption and Raman spectroscopy studies of InSbBi layers grown by liquid phase epitaxy. Infrared Phys Techn 55(4):306–308
24. Rajpalke MK, et al (2014) Bi-induced band gap reduction in epitaxial InSbBi alloys. Appl Phys Lett 105(21):212101
25. Sweeney SJ, Jin SR (2013) Bismide-nitride alloys: promising for efficient light emitting devices in the near- and mid-infrared. J Appl Phys 113(4):043110
26. Occena J, Jen T, Rizzi EE, Johnson TM, Horwath J, Wang YQ, Goldman RS (2017) Bi-enhanced N incorporation in GaAsNBi alloys. Appl Phys Lett 110(24):242102
27. Su M, Li C, Yuan P, Rao F, Jia Y, Wang F (2014) Electronic and optical properties of quaternary alloy GaAsBiN lattice-matched to GaAs. Opt Express 22(25):30633–30640
28. Jin S, Sweeney SJ (2013) InGaAsBi alloys on InP for efficient near- and mid-infrared light emitting devices. J Appl Phys 114(21):213103
29. Petropoulos JP, Zhong Y, Zide JMO (2011) Optical and electrical characterization of InGaBiAs for use as a mid-infrared optoelectronic material. Appl Phys Lett 99(03):031110
30. Luo G, Forghani K, Kuech TF, Morgan D (2016) First-principles predictions of electronic properties of $GaAs_{1-x-y}P_yBi_x$ and $GaAs_{1-x-y}P_yBi_x$-based heterojunctions. Appl Phys Lett 109(11):112104
31. Kohn W, Sham LJ (1965) Self-consistent equations including exchange and correlation effects. Phys Rev 140(4A):1133–1138
32. Fabien CAM, Gunning BP, Doolittle WA, Fischer AM, Wei YO, Xie H, Ponce FA (2015) Low-temperature growth of InGaN films over the entire composition range by MBE. J Cryst Growth 425:115–118
33. Kresse G, Furthmüller J (1996) Efficient iterative schemes for ab initio total-energy calculations using a plane-wave basis set. Phys Rev B 54(16):11169–11186
34. Kresse G, Furthmüller J (1996) Efficiency of ab-initio total energy calculations for metals and semiconductors using a plane-wave basis set. Comp Mater Sci 6(1):15–50
35. Blöchl PE (1994) Projector augmented-wave method. Phys Rev B 50(24):17953–17979
36. Kresse G, Joubert D (1999) From ultrasoft pseudopotentials to the projector augmented-wave method. Phys Rev B 59(3):1758–1775
37. Perdew JP, Burke K, Ernzerhof M (1996) Generalized gradient approximation made simple. Phys Rev Lett 77(18):3865–3868
38. Tran F, Blaha P (2009) Accurate band gaps of semiconductors and insulators with a semilocal exchange-correlation potential. Phys Rev Lett 102(22):226401
39. César M, Ke Y, Ji W, Guo H, Mi Z (2011) Band gap of $In_xGa_{1-x}N$: a first principles analysis. Appl Phys Lett 98(20):202107
40. Haq BU, Ahmed R, Shaari A, Hassan FEH, Kanoun MB, Goumri-Said S (2014) Study of wurtzite and zincblende GaN/InN based solar cells alloys: First-principles investigation within the improved modified Becke-Johnson potential. Sol Energy 107:543–552
41. Onen A, Kecik D, Durgun E, Ciraci S (2016) GaN: From three- to two-dimensional single-layer crystal and its multilayer van der Waals solids. Phys Rev B 93(8):085431
42. Schulz H, Thiemann KH (1977) Crystal structure refinement of AlN and GaN. Solid State Commun 23(11):815–819
43. García R, et al (2002) A novel method for the synthesis of sub-microcrystalline wurtzite-type $In_xGa_{1-x}N$ powders. Mat Sci Eng B 90(1-2):7–12
44. Morales FM, et al (2009) Determination of the composition of $In_xGa_{1-x}N$ from strain measurements. Acta Mater 57(19):5681–5692
45. Cordero B, Gómez V, Platero-Prats AE, Revés M, Echeverría J, Cremades E, Barragán F, Alvarez S (2008) Covalent radii revisited. Dalton Trans 0(21):2832–2838
46. Moses PG, Miao M, Yan Q, Van de Walle CG (2011) Hybrid functional investigations of band gaps and band alignments for AlN, GaN, InN, and InGaN. J Chem Phys 134(8):084703
47. Magnuson M, Mattesini M, Höglund C, Birch J, Hultman L (2010) Electronic structure of GaN and Ga investigated by soft X-ray spectroscopy and first-principles methods. Phys Rev B 81(8):085125
48. Dingle R, Sell DD, Stokowski SE, Ilegems M (1971) Absorption, reflectance, and luminescence of GaN epitaxial layers. Phys Rev B 4(4):1211–1218
49. Ilegems M, Dingle R, Logan RA (1972) Luminescence of Zn- and Cd-doped GaN. J Appl Phys 43(9):3797–3800
50. Davydov VY, et al (2002) Band gap of InN and In-Rich $In_xGa_{1-x}N$ alloys ($0.36 < x < 1$). Phys Stat Sol (b) 230(2):4–6
51. Kim M-H, Cho J-K, Lee I-H, Park S-J (1999) Metalorganic molecular beam epitaxy of InGaN layers and their optical properties. Phys Stat Sol (a) 176(1):269–272
52. Lu P, Liang D, Chen Y, Zhang C, Quhe R, Wang S (2017) Closing the bandgap for III-V nitrides toward mid-infrared and THz applications. Sci Rep 7:10594
53. Shi J, Zhang S, Yang M, Zhu S, Zhang M (2011) Light emission from several-atom In-N clusters in wurtzite Ga-rich InGaN alloys and InGaN/GaN strained quantum wells. Acta Mater 59(7):2773–2782